Physics of brain dynamics: Fokker–Planck analysis reveals changes in EEG δ–θ interactions in anæsthesia

Physics of brain dynamics: Fokker–Planck analysis reveals changes in EEG δ–θ interactions in anæsthesia

A Bahraminasab[1], **F Ghasemi**[2], **A Stefanovska**[1,3],
P V E McClintock[1] **and R Friedrich**[2]

[1] Department of Physics, Lancaster University, Lancaster LA1 4YB, UK
[2] Institute of Theoretical Physics, Westfälische Wilhelms-Universität
Wilhelm-Klemm-Strasse 9, 48149 Münster, Germany
E-mail: aneta@lancaster.ac.uk

Abstract. We use drift and diffusion coefficients to reveal interactions between different oscillatory processes underlying a complex signal and apply the method to EEG δ and θ frequencies in the brain. By analysis of data recorded from rats during anæsthesia, we consider the stability and basins of attraction of fixed points in the phase portrait of the deterministic part of the retrieved stochastic process. We show that different classes of dynamics are associated with deep and light anæsthesia, and we demonstrate that the predominant directionality of the interaction is such that θ drives δ.

[3] Author to whom any correspondence should be addressed.

IOP Institute of Physics ⦿ DEUTSCHE PHYSIKALISCHE GESELLSCHAFT

Contents

1. Introduction

Complex signals typically contain a great deal of information about the underlying processes that generate them, but the extraction of such information can be difficult and requires methods drawn from physics and nonlinear science [1]–[4]. This is especially true of signals derived from living systems. Their complexity arises in part from nonlinear interactions between subsystems oscillating on widely differing timescales, and in part from the confusing influence of seemingly random fluctuations. Electroencephalographic (EEG) recordings of brain activity [1] exemplify the problem. It has long been appreciated [5] that they exhibit continuous widespread oscillations, but their origin remains barely understood. As in the case of cardiovascular signals [6], there are multiple rhythms enclosed within broad-band noise. In dynamical terms, these oscillations might be attributed to limit-cycle attractors, because analyses of short segments often reveal spectral peaks in particular frequency ranges. Interactions between the processes generating some of these EEG waves have been demonstrated [7] but not yet explored much.

Understanding the interdependences between complex dynamical systems is of quite general scientific importance, e.g. in physics, chemistry, biology and neuroscience; it can also be of importance for, e.g. economics and sociology. Often, the underlying equations of motion are unknown, but a detailed quantitative description of interdependences can nonetheless be achieved by time-series analysis of experimentally measured observables. In recent years, a number of methods have been developed that allow one to detect and to quantify the strengths of the possible interactions [8]. Asymmetric approaches have facilitated the detection of directional coupling from time series. At some risk of over-simplification they can conveniently be divided into three main groups: techniques based on interrelationships between parameters of oscillatory dynamics and, in particular, phase dynamics [9]–[11]; state-space-based methods [12, 13] and information-theoretic approaches [14, 15].

State-space-based approaches provide strong methods for detecting generalized synchronization or directionality patterns between two coupled systems. Also, the fact that there are not many free parameters involved in driving the state-space patterns makes such measures relatively easy to implement, and robust. Their main challenges are in finding well-defined quantitative measures of directionality or driver-response and in that it is often difficult to localize the reconstructed properties in time. Generally, all three groups of methods tend
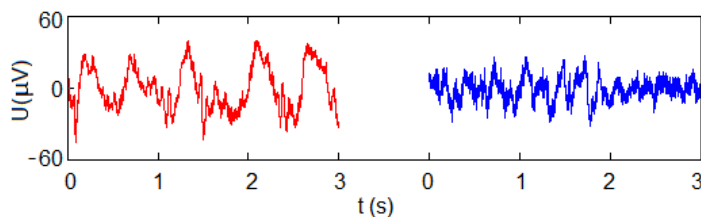
Figure 1. Short (3 s) segments of EEG signal for deep (left) compared with light (right) anæsthesia.

to make rather strict assumptions about the dynamics of the systems that generate the time series, e.g. that they should be linear systems, or in the case of self-sustained oscillators that they should be weakly-coupled. Furthermore, many of the approaches focus preferentially on the low-dimensional deterministic part of the dynamics. In reality, however, the influences of noise on nonlinear dynamical systems can be far from trivial [16]–[18] and they constitute a subject of continuing interest and importance. Real signals frequently result from dissipative dynamical systems under the influence of noise, and it is often useful to describe them in terms of Fokker–Planck formalism [19].

In this paper, we combine the multidimensional Fokker–Planck equation [16, 20] with mathematical modelling of the system dynamics, enabling us to extract model parameters directly from the measured time series [2, 3, 20]. We concentrate on the interactions between EEG θ waves and δ waves in anæsthesia, and characterize some of their properties. Following [20, 21] we apply a two-dimensional (2D) Markov analysis to EEG signals recorded [22] from rats during deep and light anæsthesia (see examples in figure 1); and we carry out a stability analysis of the deterministic part of the derived equations. We find in these experiments that the dynamics falls into different universality classes for the states of deep and light anæsthesia, enabling us to distinguish robustly between them. Although we treat brain dynamics explicitly, the method is applicable to complex systems quite generally.

In section 2, we describe succinctly how our experimental data were acquired from rats and pre-processed prior to analysis. Section 3 describes the basic method used for the analysis, and section 4 discusses how we applied it to the rat EEG signals and considers the results that emerge. Section 5 describes some simple tests undertaken to eliminate artifacts and to check the validity of the results. Finally, in section 6, we summarize and consider the main results, and draw conclusions.

2. Experimental methods and data acquisition

A full description of how the signals were measured has already been given elsewhere [22], so here we just summarize the salient features. The experiments were performed on 10 adults, male Wistar rats weighing 250–300 g. The animals were each anæsthetized with a single intraperitoneal injection of ketamine hydrochloride (45 mg (kg body wt)$^{-1}$) and xylazine hydrochloride (7 mg (kg body wt)$^{-1}$). (Measurements were also carried out on a second group of rats anæsthetized with pentobarbital [22] but these are not discussed here.) As soon as the rat could no longer hold its upright posture, 10–15 min after administration of the drug, it was placed in a darkened Faraday cage where sensors were mounted and recording

started immediately. The EEG was recorded over the left and right parietal cortex with three hypodermic needles inserted under the animal's scalp to serve as electrodes. The EEG was differentially amplified by $10^3 \times$ and low-pass filtered with a cut-off frequency of 300 Hz. The resultant signal was fed through a signal conditioning system, digitized at 1 kHz with 16-bit resolution, and stored on the hard disk of a laptop computer.

Depth of anaesthesia was assessed at 5 min intervals by a nociceptive stimulus, the skin-pinch test, applied to the sole of the animal's front paw [23]. The recording started with a negative test response, i.e. when the rat stopped responding with a reflex withdrawal of the limb. The monitoring was terminated on the reappearance of a positive pinch-test response, as the animal immediately started to move thereby terminating reliable data recording. The duration of recording varied from rat to rat and was on average 87 min. The measurements were at a constant room temperature of $24 \pm 1\,°C$.

The EEG power spectrum is conventionally divided [24] into the frequency bands: δ (0.5–3.5 Hz); θ (3.5–7.5 Hz); α (7.5–12.5 Hz); β (12.5–25 Hz); γ_1 (25–35 Hz); γ_2 (35–50 Hz); and γ_3 (50–100 Hz). We calculated the time evolution within each band by application of the continuous wavelet transform [6]. The EEG signal was bandpass-filtered, but only after extensive investigation of its time-frequency content by wavelet analysis, and particular care taken to avoid any introduction of phase lags.

The transition from deep to light anaesthesia was determined by application of several criteria: as the times when both cardiac and respiratory frequencies significantly increased and became significantly more variable [22]; as the times when the amplitude of δ-waves dramatically decreased; and as the times when the amplitudes of θ and γ significantly increased. These different criteria yielded consistent results. The transition is most probably associated with the effects of the ketamine wearing off faster that those of xylazine so that in the light phase the effect of xylazine is dominant.

3. Fokker–Planck analysis

We define a state vector $\mathbf{q} = \{\delta(t), \theta(t)\}$ composed of the signals of the δ and θ bands, hypothesize that it follows a stochastic process of form

$$\partial_t q_i = D_i^{(1)}(\mathbf{q}, t) + \sum_{j=1}^{2} \sqrt{D_{ij}^{(2)}(\mathbf{q}, t)}\, \Gamma_j(t),$$

and approximate the fluctuations $\Gamma_j(t)$ by Gaussian white noise. We suppose that the process is Markovian, an assumption that can subsequently be validated by data analysis. The drift vector $\mathbf{D}^{(1)}$ describing the deterministic part of the dynamics, and the diffusion matrix $\mathbf{D}^{(2)}$ determining the strength of the driving noise, are

$$D_i^{(1)}(\mathbf{q}, t) = \lim_{\tau_M \to 0} \frac{1}{\tau_M} \langle (q_i(t + \tau_M) - q_i(t)) \,|\, \mathbf{q}, t \rangle,$$

$$D_{ij}^{(2)}(\mathbf{q}, t) = \lim_{\tau_M \to 0} \frac{1}{2\tau_M} \langle (q_i(t + \tau_M) - q_i(t))(q_j(t + \tau_M) - q_j(t)) | \mathbf{q}, t \rangle.$$

(1)

We have used the Itô interpretation of the stochastic integral and conditional expectation values $\langle \cdot \rangle$ that can be determined from the experimental data; $\sqrt{\mathbf{D}^{(2)}}$ is to be calculated by diagonalizing the matrix $\mathbf{D}^{(2)}$, taking the square root of each of its elements, and transforming the result back into the original system of coordinates [16].
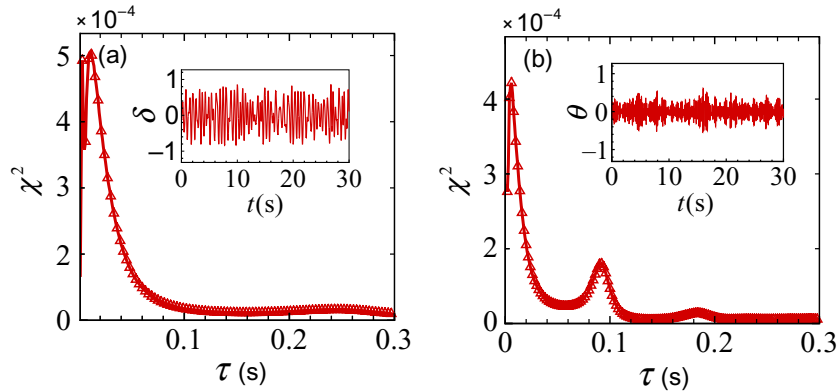
Figure 2. Plots of χ^2 to test the Markov property of (a) δ and (b) θ fluctuations in a rat's EEG as a function of timescale, τ. The minimum value of χ^2 occurs around $\tau_M \simeq 0.1$ s, corresponding to the Markov timescale within a σ confidence level. The insets plot short samples of the signals being analysed.

The Markov condition requires an n-point conditional probability function (CPF) $P(\mathbf{q}(t + n\tau)|\mathbf{q}(t + (n-1)\tau), \ldots, \mathbf{q}(t+\tau), \mathbf{q}(t))$ to be equal to a two-point CPF $P(\mathbf{q}(t+n\tau)|\mathbf{q}(t + (n-1)\tau))$. The timescale τ in which this condition is fulfilled is the *Markov timescale* (τ_M). For multidimensional stochastic variables, it is hardly possible to check the Markov condition directly by means of n-point CPFs. We therefore use three-point CPFs, for which the Markov condition corresponds [25] to

$$\chi^2 = \int \left(\prod_{i=1}^{3} dx_i \right) \frac{[P(x_3, x_2, x_1) - P(x_3|x_2)P(x_2, x_1)]^2}{\sigma_J^2 + \sigma_M^2} \tag{2}$$

being zero. Here,

$$x_3 = x_3(t + 2\tau), \quad x_2 = x_2(t + \tau), \quad x_1 = x_1(t),$$

and x represents one of the components of $\mathbf{q}$, i.e. q_i. σ_J^2 and σ_M^2 are the variances of $P(x_3, x_2, x_1)$ and $P(x_3|x_2)P(x_2, x_1)$, respectively. Figure 2 shows χ^2 calculated for both δ and θ waves from a rat EEG signal as a function of the timescale τ. In both cases, the minimum value of χ^2 occurs just after 0.1 s, after which it hardly changes, corresponding to τ_M with one σ confidence level.

Using equation (1) with this value of τ_M, we can estimate the drift and diffusion coefficients from $\delta(t)$ and $\theta(t)$ as shown in figure 3. In doing so, we used 1D coefficients, i.e. in deriving the drift and diffusion coefficients for each variable, the effect of the other variable was integrated. Both coefficients can be well-approximated by low-order polynomials. The $D_i^{(1)}$ with $i = \delta, \theta$ indicate an overall damping behaviour, as shown earlier [26]. Moreover, the behaviour of $D_{\delta\delta}^{(2)}$ and $D_{\theta\theta}^{(2)}$ implies that the noise is multiplicative in character: constant diffusion coefficients represent additive noise whereas, for multiplicative noise, the diffusion coefficients are functions of the dynamical variables. We tested whether the deviation from additive behaviour is attributable to the finiteness of τ_M [27] by consideration [28] of a Taylor expansion of the drift coefficients. We conclude that the effect of the higher order terms in τ_M cannot explain the apparently multiplicative nature of the estimated second coefficient, which implies that the noise strengths are functions of the dynamical variables.
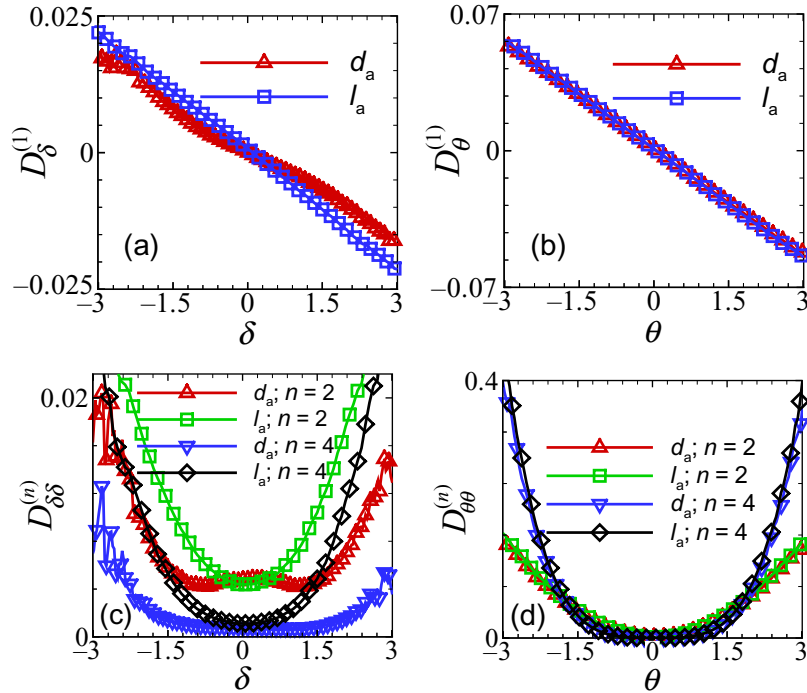
Figure 3. Plots of the derived drift, diffusion and fourth-order Kramers–Moyal coefficients for the EEG of a typical rat in the deeply and lightly anæsthetized states (indicated by d_a and l_a, respectively). (a) Drift coefficient for the EEG δ band. (b) Drift coefficient for the θ band. (c) Diffusion and fourth-order Kramers–Moyal coefficients related to the δ band. (d) Diffusion and fourth-order Kramers–Moyal coefficients related to the θ band. The results of (a) and (c) clearly demonstrate different functionality for both the drift and diffusion coefficients during deep as compared with light anæsthesia.

4. Application to δ and θ brain waves in anæsthesia

Figures 3(a) and (c) show that there are significant differences in the δ waves between deep and light anæsthesia, consistent with earlier work [22]. On the other hand, panels (b) and (d) show that little change occurs in the θ waves. The functionality of $D_{\delta\delta}^{(2)}$ changes markedly between the two states as can be seen in figure 3(c): in the light phase, a parabola fits this coefficient very well, while for deep anæsthesia we must use a fourth-order function to describe the central peak.

4.1. Stationary solution for retrieved drift and diffusion coefficients

We can also examine qualitatively the stationary solution of the Fokker–Planck equation around the different extrema in $D_2(\delta)$. The solution is $P_{\text{stationary}} = \frac{N_0}{D^2(\delta)} \exp(- \int d\delta \frac{D^{(1)}}{D^{(2)}})$, where the integration constant N_0 can be derived by normalization of $P_{\text{stationary}}$. For simplicity, we suppose that $D_{\delta}^{(1)}$ is well approximated by a line ($D_{\delta}^{(1)} = -b\delta$ where $b > 0$). In light anæsthesia, $D_{\delta\delta}^{(2)}$ has a minimum at $\delta = 0$, whereas in the deep state there is a local maximum there. Focusing on

the region around this point, $D_{\delta\delta}^{(2)}$ can be approximated as $D_{\delta\delta}^{(2)} \simeq D_{\delta\delta}^{(2)}(0) \mp \frac{1}{2}|D_{\delta\delta}^{(2)''}|\delta^2$, where $'$ denotes d/dδ. It is evident that the contribution of $D_{\delta\delta}^{(2)}$ to the stationary solution of the Fokker–Planck equation changes between deep and light anæsthesia. Two additional extrema (minima) appear in $D_{\delta\delta}^{(2)}$ during deep anæsthesia (figure 3(c)), causing a double-humped PDF in deep anæsthesia (cf the single-humped PDF during light anæsthesia).

To test whether the behaviour of the system deviates from a Langevin description, we calculated the fourth-order coefficients $D^{(4)}(x) = \lim_{\tau_M \to 0} \frac{1}{24\tau_M}\langle(x(t+\tau) - x(t))^4\rangle$ for $x = \delta$ and θ, allowing us to determine whether the driving noise process $\Gamma_j(t)$ exhibits deviations from a Gaussian distribution [16]. Only if $D^{(4)}$ vanishes is $\Gamma_j(t)$ white Gaussian. The probability density function (PDF) of the process then evolves according to a Fokker–Planck or, equivalently, Langevin equation [16]. Figure 3 shows that $D_\delta^{(4)}$ is slightly above zero, but the magnitude of this coefficient is less than one-fifth of the second coefficient $D_{\delta\delta}^{(2)}$, for both deep and light anæsthesia. The fluctuations for the case of light anæsthesia are larger than for the deep state. This can be seen from the observation that, in the domain of $[-3\sigma, 3\sigma]$ in figure 3(c), the $D_\delta^{(4)}$ terms are bigger in the light case, which indicates greater fluctuation amplitude. In contrast, for the θ band signals, $D_\theta^{(4)}$ compared with $D_{\theta\theta}^{(2)}$ was clearly above zero for both deep and light anæsthesia suggesting that a 1D Langevin description may be inadequate for modelling δ–θ activities.

In a 1D Langevin model, the effects of other components are integrated, e.g. the 2D drift and diffusion coefficients can be integrated to yield the 1D ones as $D_i^{(1)}(x_i') = \int D_i^{(1)}(x_i, x_j)P(x_i|x_i', x_j)\mathrm{d}x_j$ and $D_{ii}^{(2)}(x_i') = \int D_{ii}^{(2)}(x_i, x_j)P(x_i|x_i', x_j)\mathrm{d}x_j$. Obviously, the information about interactions and their directionality is lost. This is an important point: although we have clearly different functionality for $D_{\delta\delta}^{(2)}$ and a different pattern for $D_\delta^{(1)}$, the differences are unclear in the case of the θ component and we should not thoughtlessly integrate out the effects of the other variable. So, next, we derive the drift and diffusion coefficients as functions of both δ and θ. Figure 4 shows all the coefficients calculated for deep anæsthesia. Figures 4(a) and (b) plot $D_\delta^{(1)}(\delta, \theta)$ and $D_\theta^{(1)}(\delta, \theta)$. The θ-component of the drift vector shows an almost linear dependence on θ and only weak variations with δ. But interestingly, the δ-component of the drift vector has strong functionality in both δ and θ (see figure 4(a)). We used a 2D least-squares method to derive the functionality of the coefficients. In the case of θ, we have $D_\theta^{(1)}(\delta, \theta) = a + b\delta + c\theta$ with good precision and the value of b is small ($|c/b| \simeq 10$ for all rats), while in the case of δ the situation changes dramatically. The best fit available is a third-order polynomial with respect to δ and θ, $D_\delta^{(1)}(\delta, \theta) = \sum_{m,n} a_n^m \delta^m \theta^n (m + n = 0, 1, 2, 3)$. In figures 4(c) and (d), we plot the coefficients $D_{\delta\delta}^{(2)}$ and $D_{\theta\theta}^{(2)}$ of the diffusion matrix. It is evident that $D_{\theta\theta}^{(2)}$, like $D_\theta^{(1)}$, depends weakly on δ. In both cases, a second-order polynomial of δ and θ such as $\sum_{m,n} a_n^m \delta^m \theta^n (m + n = 0, 1, 2)$ can describe the functionality of the two diffusion components. In case of light anæsthesia, we find similar functionality albeit with different parameters for the diffusion coefficients; but we find different functionality for the δ-component of the drift coefficient, which has a much weaker dependence on θ. It was found that these same patterns were repeated for all ten rats. Thus, they can be used to characterize the dynamical behaviour of the δ and θ brain activities.

The fact that $D_\delta^{(1)}$ and $D_{\delta\delta}^{(2)}$ have strong dependence on both δ and θ, whereas the $D_\theta^{(1)}$ and $D_{\theta\theta}^{(2)}$ hardly vary at all with δ, shows that the EEG θ component influences the δ-component but not vice versa. This situation persists regardless of depth of anæsthesia.
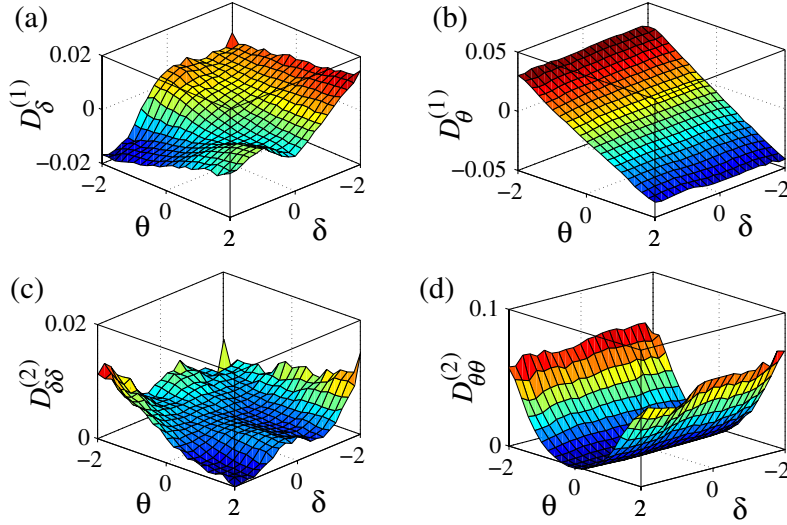
Figure 4. 2D drift, diffusion and fourth-order Kramers–Moyal coefficients for the deeply anæsthetized state of the same rat as in figure 3. (a) Drift coefficient for the EEG δ band and (b) for the θ band. (c) The $\delta\delta$-component of the diffusion matrix and (d) its $\theta\theta$-component. In all four figures, the amplitudes are increasing from dark blue to dark red. $D_\delta^{(1)}$ and $D_{\delta\delta}^{(2)}$ have strong dependences on both δ and θ, whereas the dependence of $D_\theta^{(1)}$ and $D_{\theta\theta}^{(2)}$ on δ is weak.

4.2. Dynamics and fixed points (FPs)

To complete the analysis we need to derive a more quantitative description of the patterns appearing in the drift and diffusion coefficients. The generated Langevin equations give the deterministic and stochastic parts of dynamics, which can be written as $\partial_t q_i = \partial_t^D q_i + \partial_t^S q_i$, of which $\partial_t^D q_i = D_i^{(1)}$ is the deterministic part of the dynamics and $\partial_t^S q_i = \sum_{j=1}^2 \sqrt{D_{ij}^{(2)}} \Gamma_j$. Because of the finite noise we do not have clear control of the stochastic term so, for simplicity, we just compare the dynamics arising from the deterministic terms: we can derive the FPs and the stability exponents in the phase diagram from the deterministic parts of the δ and θ trends. We note that another way to determine asymmetries in coupling is from measures based on the drift and diffusion coefficients [29].

In carrying out these analyses, we used all data we had for each rat [22], i.e. for a measurement of duration 30 min we had $30 \times 60 \times 1000 = 1.8 \times 10^6$ sample data for our sampling frequency of 1000 Hz. Thus the results related to $D^{(1)}$, $D^{(2)}$, and $D^{(4)}$ are all supported by a good level of statistics. However, we have also checked our results by using different portions of data. We found that 5 min worth of data (300 k data samples) was sufficient to give us a robust estimation of $D^{(1)}$, $D^{(2)}$ and $D^{(4)}$. In relation to the Markov length scale τ_M we found that, although the results were obtained for $\tau_M = 0.1$ (100 sample data), a range of 80–120 samples gave the same results. Diverging from this range, however, would drive us into a regime where modelling based on the Markov process is no longer valid.

To examine the FPs and flows in the δ–θ phase space, we have to solve together:

$$\partial_t^D q_\delta = D_\delta^{(1)}(\delta, \theta),$$
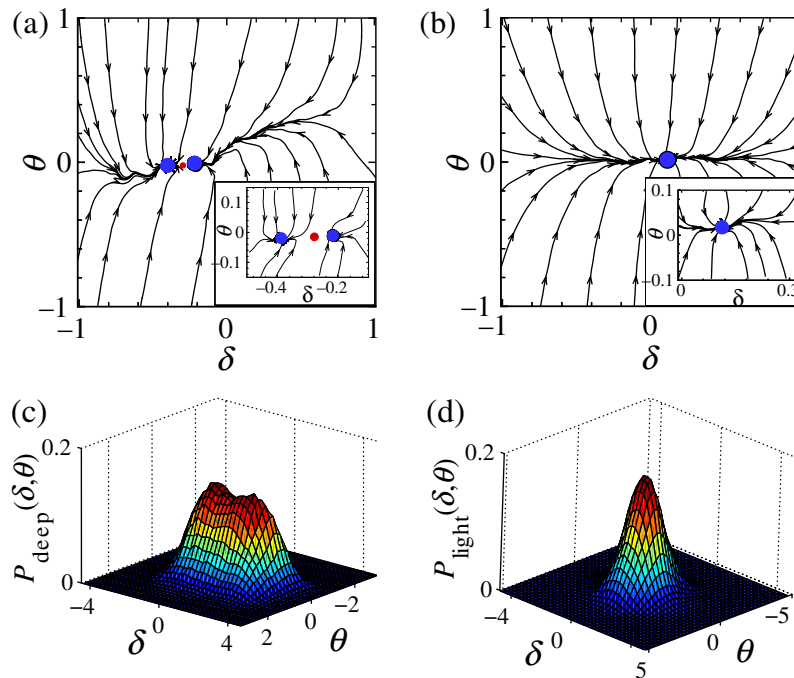$$\partial_t^D q_\theta = D_\theta^{(1)}(\delta, \theta),$$

(3)

Figure 5. Comparison of the flow diagrams related to (a) deep and (b) light anæsthesia, derived from the deterministic part of the dynamics. Insets show in more detail the areas around the stable FPs (shown as blue dots) and unstable fixed point (red dot). The figure illustrates the different universality classes corresponding to deep and light anæsthesia. (c) and (d) show the joint PDF for deep and light regimes, $P_{\mathrm{deep}}(\delta, \theta)$ and $P_{\mathrm{light}}(\delta, \theta)$, respectively. The PDFs are evidently consistent with the results derived from the stability analyses shown in (a) and (b). The amplitudes of PDF plots are increasing from minimum in dark blue (zero) to maximum value at dark red.

for both deep and light anæsthesia. We find that there are two distinct regimes. Firstly, for eight out of ten rats during deep anæsthesia there are three nontrivial FPs. Two of them are stable in both the δ and θ directions, and the third one is unstable in the δ but stable in the θ direction. Figure 5(a) shows the flow diagrams related to equation (3) for a typical rat. There is a region outside the two stable FPs in δ–θ space in which the flows take any initial point to one of the stable FPs. However, when δ or θ are small enough that the initial point is close to the unstable fixed point, a small change in δ could take the flow to a different stable fixed point, hence implying that the joint PDF of the δ and θ, $P_{\mathrm{deep}}(\delta, \theta)$, must have two distinctive peaks. Secondly, for all ten rats during light anæsthesia, we have only one attracting FP. Figure 5(b) shows that, for a typical rat, over the whole interval of δ and θ flows take any initial point to the stable fixed point. Hence, in this case, the system appears homogeneous at large timescales and we must have one peak for $P_{\mathrm{light}}(\delta, \theta)$, unlike the previous case. To test this prediction, we plot in figures 5(c) and (d) the directly calculated PDFs $P_{\mathrm{deep}}(\delta, \theta)$ and $P_{\mathrm{light}}(\delta, \theta)$. They are in full agreement with the results of our stability analysis of drift coefficients. At least in the present experiments, therefore, we may conclude that the dynamics of δ–θ activity falls into different universality classes for the states of deep and light anæsthesia. However, this finding needs further investigation and will be a subject of our future work.

5. Tests of the validity of the results

We now describe some tests that we carried out to confirm that our results relate to the real dynamics of the system, and are not just artifacts of filtering. To do so, we processed a dummy signal consisting of Ornstein–Uhlenbeck noise [30] by filtration in the δ and θ bands and then repeated the whole analysis procedure. We used standard Ornstein–Uhlenbeck noise with an added sinusoidal interaction to simulate the external oscillatory components. The equation for the dynamical variable is

$$\dot{v} = -v(t) + A\sin(\omega t) + \sqrt{\xi}\,\eta(t) \tag{4}$$

where A corresponds to the coupling strength of the external oscillatory components, ξ is the noise strength, and η is the white Gaussian noise.

We always obtained one attracting FP, implying the damping structure of the system. Moreover, when analysing the empirical data with 5 min moving windows for the δ and θ bands of the real signals, we observed that the change of pattern between deep (3 FPs) to light (1 FP) anæsthesia occurs very sharply: we estimated the $D^{(1)}$, $D^{(2)}$ for one window of data, and then repeated the whole process explained in sections 4.1 and 4.2 by first deriving the functionality of $D^{(1)}$ and $D^{(2)}$ based on the dynamical variables, and then applying stability analysis to the deterministic parts of the processes (similar to the procedure explained in section 4.2). Interestingly we found that even with the short 5 min data windows, we could distinguish clearly between two different phases, having 3 and 1 FPs for deep and light anæsthesia, respectively, the transition from one to the other being related to the transition from deep to light anæsthesia, which occurs very sharply ($\sim$1–2 min).

Finally, we investigated the question of whether or not the same results can be derived from the phase dynamics of the variables δ and θ. We used the Hilbert transform [31] to detect the corresponding phases; we calculated the time interval for each period of the phase; and we inverted these time series to derive new signals in frequency space. Note that the phases of δ and θ are defined only in a statistical sense because both waves are relatively broad in frequency. It is only δ waves in deep anaesthesia that are relatively localized in frequency. For further details see [22].

We then processed the δ and θ phases using the Fokker–Planck formalism. Reassuringly, but unsurprisingly, there were no significant differences between the drift and diffusion coefficients corresponding to the δ and θ phases in deep and light anæsthesia (not shown here).

6. Concluding remarks

In conclusion, our Fokker–Planck analysis of EEG signals has provided evidence of interactions between the EEG δ and θ wave activities in rats in deep and light anæsthesia. We have characterized the functionalities of δ and θ and shown that the functionality of δ alters with changes in depth of anæsthesia. It is commonly accepted that sleep or anaesthetic-induced unconsciousness arises through changes in the conduction of ion channels. Ketamine inhibits [32] NMDA[4] and Muscarinic ACh-sensitive[5] channels, which may occur through two

---

[4] NMDA stands for N-methyl D-aspartate. Activation of NMDA receptors results in the opening of the ion channel.

[5] ACh stands for acetylcholine. Activation of Muscarinic ACh-sensitive receptors results in the opening of the ion channel.

distinct mechanisms: (i) ketamine blocks open channels thereby reducing their mean open time; or (ii) it decreases the frequency of channel opening. Either mechanism would lead to neuronal hyperpolarization and reduce the activation of action potentials. The consequence of the hyperpolarization is that the function of neurons is blocked. Where exactly this occurs is currently unknown. Specific suppression of activity in the regional-thalamic and mid-brain reticular formation and hyperpolarization blockage of thalamocortical neurons has been discussed [33]. On the other hand, ketamine is considered as a drug that does not reduce cortical metabolism and glutamate release or depress sensory information flow through the thalamus [34]. Our observation that θ drives δ, regardless of depth of anæsthesia is consistent with this picture. It is an important result, suggesting that the changes in δ-activity during deep anæsthesia or sleep are mainly due to reduced sensory information from the spinal cord to the thalamus, rather than on account of reduced thalamocortical interactions. However, the physiological and neurological implications of this finding remain to be further investigated.

Acknowledgments

References

[1] Freeman W J, Kozma R and Werbos P J 2001 Biocomplexity: adaptive behavior in complex stochastic dynamical systems *Biosystems* **59** 109–23
[2] Kantz H and Schreiber T 2003 *Nonlinear Time Series Analysis* (Cambridge: Cambridge University Press)
[3] Boccara N 2004 *Modeling Complex Systems* (Berlin: Springer)
[4] Caruso A, Gargano M E, Valenti D, Fiasconaro A and Spagnolo B 2005 Cyclic fluctuations, climatic changes and role of noise in planktonic foraminifera in the Mediterranean sea *Fluctuation Noise Lett.* **5** L349–55
[5] Berger H 1929 Ueber das Elektroenkephalogramm des Menschen *Arch. Psychiatr. Nervenkr.* **87** 527–70
[6] Stefanovska A and Bračič M 1999 Physics of the human cardiovascular system *Contemp. Phys.* **40** 31–55
[7] Gans F, Schumann A Y, Kantelhardt J W, Penzel T and Fietze I 2009 Cross-modulated amplitudes and frequencies characterize interacting components in complex systems *Phys. Rev. Lett.* **102** 098701
[8] Hlavackova-Schindler K, Paluš M, Vejmelka M and Bhattacharya J 2007 Causality detection based on information-theoretic approaches in time series analysis *Phys. Rep.* **441** 1–46
[9] Cimponeriu L, Rosenblum M and Pikovsky A 2004 Estimation of delay in coupling from time series *Phys. Rev.* E **70** 046213
[10] Jamšek J, Stefanovska A, McClintock P V E and Khovanov I A 2003 Time-phase bispectral analysis *Phys. Rev.* E **68** 016201
[11] Smelyanskiy V N, Luchinsky D G, Stefanovska A and McClintock P V E 2005 Inference of a nonlinear stochastic model of the cardiorespiratory interaction *Phys. Rev. Lett.* **94** 098101
[12] Arnhold J, Grassberger P, Lehnertz K and Elger C E 1999 A robust method for detecting interdependences: application to intracranially recorded EEG *Physica* D **134** 419–30
[13] Romano M C, Thiel M, Kurths J and Grebogi C 2007 Estimation of the direction of the coupling by conditional probabilities of recurrence *Phys. Rev.* E **76** 036211
[14] Schreiber T 2000 Measuring information transfer *Phys. Rev. Lett.* **85** 461–4

[15] Paluš M and Stefanovska A 2003 Direction of coupling from phases of interacting oscillators: an information-theoretic approach *Phys. Rev.* E **67** 055201

[16] Risken H 1984 *The Fokker–Planck equation* (Berlin: Springer)

[17] Moss F and McClintock P V E (ed) 1989 *Noise in Nonlinear Dynamical Systems* vol 1–3 (Cambridge: Cambridge University Press)

[18] Siegert S, Friedrich R and Peinke J 1998 Analysis of data sets of stochastic systems *Phys. Lett.* A **243** 275–80

[19] Risken H 1993 *The Fokker–Plank Equation* 2nd edn (Berlin: Springer))

[20] Friedrich R, Peinke J and Renner C 2000 How to quantify deterministic and random influences on the statistics of the foreign exchange market *Phys. Rev. Lett.* **84** 5224–7

[21] Friedrich R, Siegert S, Peinke J, Luck S, Siefert M, Lindemann M, Raethjen J, Deuschl G and Pfister G 2000 Extracting model equations from experimental data *Phys. Lett.* A **271** 217–22

[22] Musizza B, Stefanovska A, McClintock P V E, Paluš M, Petrovčič J, Ribarič S and Bajrović F F 2007 Interactions between cardiac, respiratory and EEG-δ oscillations in rats during anæsthesia *J. Physiol.* **580** 315–26

[23] Bajrović F and Sketelj J 1998 Extent of nociceptive dermatomes in adult rats is not primarily maintained by axonal competition *Exp. Neurol.* **150** 115–21

[24] John E R 2002 The neurophysics of consciousness *Brain Res. Rev.* **39** 1–28

[25] Ghasemi F, Bahraminasab A, Movahed M S, Rahvar S, Sreenivasan K R and Tabar M R R 2006 Characteristic angular scales in cosmic microwave background radiation *J. Stat. Mech.* P11008

[26] Prusseit J and Lehnertz K 2007 Stochastic qualifiers of epileptic brain dynamics *Phys. Rev. Lett.* **98** 138103

[27] Ragwitz M and Kantz H 2001 Indispensable finite time corrections for Fokker–Planck equations from time series data *Phys. Rev. Lett.* **87** 254501

[28] Friedrich R, Renner C, Siefert M and Peinke J 2002 Comment on 'Indispensable finite time corrections for Fokker–Planck equations from time series data' *Phys. Rev. Lett.* **89** 149401

[29] Prusseit J and Lehnertz K 2008 Measuring interdependences in dissipative dynamical systems with estimated Fokker–Planck coefficients *Phys. Rev.* E **77** 041914

[30] Gardiner C W 2004 *Handbook of Stochastic Methods* (New York: Springer)

[31] Pikovsky A, Rosenblum M and Kurths J 2001 *Synchronization Universal—A Concept in Nonlinear Sciences* (Cambridge: Cambridge University Press)

[32] Alkire M T 2008 Consciousness and anesthesia *Science* **322** 876–80

[33] Alkire M T, Haier R J and Fallon J H 2000 Toward a unified theory of narcosis: brain imaging evidence for a thalamocortical switch as the neurophysiologic basis of anesthetic-induced unconsciousness *Conscious Cogn.* **9** 370–86

[34] Rudolph U and Antkowiak B 2004 Molecular and neuronal substrates for general anæsthetics *Nat. Rev. Neurosci.* **5** 709–20